applied sciences

MDPI

Article

The Study of Cooling Mechanism Design for High-Power Communication Module with Experimental Verification

Tsu-Ping Yu [1,*], Yung-Lung Lee [1], Ya-We Li [1] and Shih-Wei Mao [2]

[1] Chung Cheng Institute of Technology, National Defense University, Taoyuan City 335009, Taiwan; yunglunglee84@gmail.com (Y.-L.L.); yaweilee@ndu.edu.tw (Y.-W.L.)
[2] ROC Military Academy, Kaohsiung City 830208, Taiwan; swmao1@gmail.com
* Correspondence: johinuee0921@gmail.com

Abstract: With the continued development of 5G mobile communications technology, the implementation of high-power communication systems has become a key indicator of developed nations. Communication modules are also trending toward wide bandwidth and high-capacity Multi-Input and Multi-Output systems. As the signal transmission speed and resolution continue with the increasing trend, the power used to operate these communications systems increase, causing extreme heat generation by transmit/receive modules (T/R module). In conditions where computation load increases in micro design systems, chips must operate in environments that are narrow, sealed, and have no convection, which can drastically increase the thermal load within a system. If no proper cooling system is utilized, the system fails or operates at impacted performance due to excessive temperatures. To solve the aforementioned problem, this study aimed to optimize the design of the cooling system in the T/R modules of communications systems by integrating heat pipes, cooling fans, cooling fins, and cooling chips within a limited space. We also proposed four types of cold plates based on the different directional clamp-in configuration methods of heat pipes within copper panels and utilized the finite element method to simulate and analyze the heat dissipation performance. The simulation results reveal that cold plates of types I and II can achieve a better heat dissipation performance. Finally, types I and II cold plates were selected for production and experimental verification. The results show that heat dissipation performances were similar to simulation results. The results also confirmed that type II cold plate has a better temperature uniformity and heat transfer efficiency. Thus, the cooling mechanism depicted in this study is viable in practical applications. The proposed mechanisms can also provide a reference for heat dissipation design patterns in different electronic module settings.

Keywords: communication module; heat dissipation; heat pipe; thermo electric cooler (TEC)

Citation: Yu, T.-P.; Lee, Y.-L.; Li, Y.-W.; Mao, S.-W. The Study of Cooling Mechanism Design for High-Power Communication Module with Experimental Verification. *Appl. Sci.* **2021**, *11*, 5188. https://doi.org/10.3390/app11115188

Academic Editor: Carla Raffaelli

Received: 12 May 2021
Accepted: 31 May 2021
Published: 3 June 2021

1. Introduction

As support continues for rapid technological advancement, performance requirements for electronic products have become diverse as they are released at faster computation speeds. However, the market is more focused on safety, reliability, and product lifespan, besides the aesthetic design. Furthermore, the trend of miniaturization of electronic products and the significant increase of power in sealed spaces has resulted in the continuous increase in heat generation per unit area of components. For example, a computer's central processing unit (CPU) now provides even more number of cores to speed up data processing via division of labor. In addition to the I3, I5, and I7 released by Intel, the premium high-performance I9 has also been released. These components have increased their number of cores and multi-threading within the limited surface area and data processing, causing 32 and 64 core thread processors to generate thermal power as high as 250 W. Both CPU and other integrated circuit (IC) packages need to address the issues of increasing heat flux density and power; thus, the requirement for thermal management

came into existence. To solve the issue of heat dissipation, all types of thermal components are continually developed and launched. Currently, the most common thermal components are aluminum cooling fins, copper base aluminum cooling fins, copper cooling fins, heat pipes, flat plate heat pipes (also known as vapor chambers), directional graphite heat sinks, water-cooling heat sinks, liquid vapor heat exchangers, and other products.

The current thermal solutions for electronic components often utilize heat dissipation design mechanisms that integrate various thermal components such as cooling fins and fans. Thermal components utilize contact surfaces to transfer heat to the cooling fins and convection generated by fans and other methods to expel heat to external spaces. One of the key methods to increase thermal performance is increasing the surface area of fins and increasing the revolutions per minute of fans (amount of wind) to achieve the goal of quick heat dissipation. However, the excessive density of cooling fins increases thermal resistance. Faced with his issue, Azar and Mandrone [1] studied the relationship of cooling fin density and thermal resistance to achieve a suitable fin density, and a suitable expansion of cooling surface area could still effectively reduce thermal resistance in cooling fins. Lehmann, Wirtz, and Arvizu [2–4] also tested different fin designs to assess the effect of heat dissipation on electronic components. Other studies have also strived to improve cooling fin design [5–7] using methods such as increasing flux performance and heat dissipation surface areas to cool the massive amount of thermal energy generated by CPUs or high-performance electronic components. Likewise, Oh, Choi, Ha, and Min [8] designed a cooling fin with a different aspect ratio (AR) between the slant angle and fin while using comparative analysis under conditions of natural convection to find optimal thermal performance and observed that the conditions of slant angle at –30 degree and AR = 4.0 could achieve optimal thermal performance. As cooling fins utilize the thermal conductivity principles of solid substances for heat dissipation, their thermal performance is limited and are gradually unable to satisfy the heat dissipation requirements of high-power components. To increase thermal performance, the principle of latent heat phase transition has been applied in recent years to increase thermal exchange efficiency and generate fast thermal conductivity; heat pipes broadly apply this principle. Their basic principle is a sealed cavity with a working fluid that utilizes the continuous circulation and two-phase change of liquid–vapor and vapor–liquid convection from liquid at the endotherm and gas at the exothermal ends within the cavity. The surface of the cavity has the characteristic of rapid temperature equalization that achieves the purpose of heat transfer [9]. In 2021, Luo, Guan, Mao, Xiao, and Zeng [10] focused on utilizing miniaturize heat pipes to improve the thermal performance of laptop computers. In 2003, Kim, Won and Back [11] designed a cooling module that integrated heat pipes, cooling fins, and fans and verified the difference in the benefits of heat dissipation at different fan speeds compared with a traditional PC cooling system (fins + fans). Results showed that the integrated design of the cooling module possessed exceptional cooling performance and retained high-performance cooling even at low fan speeds. It also solved the noise issue caused by the high fan speeds of traditional cooling systems. Many scholars have also continued to study the application of heat pipe designs by exploring the selection of different materials, manufacturing controls, or type designs that can achieve a better cooling [12–17].

When faced with products that trend toward miniaturization, using single or multiple heat pipes for cooling requirements is no longer suitable in terms of space and performance. Flat plate heat pipes (vapor chambers) are products that were derived through this development. They are cooling components based on a two-dimensional heat transfer system superior in thermal conductivity and efficiency to multiple heat pipe configurations, and because they can quickly transform a point heat source into a surface heat source, the reduction of heat transfer per unit area achieves temperature equalization and avoid heat points that can cause failure or performance issues in electronic components. The flat area and heat source have a higher contact area and can effectively reduce the system's general heat resistance achieving exceptional cooling in combination with cooling fins [18]. Vapor chambers can be designed according to different requirements. Integrated cooling

plates are a sealed component that utilizes different manufacturing methods such as metal mesh sintering, trench, or thin metal films to form different capillary structures to allow for gas–liquid phase change within the internal structure's flux to transfer heat while in contact with cooling fins through capillarity. Internal clamp heat pipes are a type of cold plate that utilize several straight or curved heat pipes clamped onto metal panels to achieve high scalability at low cost. In 2020, Mansouri, Zaghlol, and Weasner [19] verified the convection performance of two different embedded heat pipe radiators in forced convection experiments, and compared with a blank heat sink, the heat dissipation performance increased by 28%. We utilized such a design in this study.

With the continued development of communications technology, high-speed transmission, communication quality, and long-distance transmission, the operating power has also increased. Therefore, most communication systems are equipped with a large number of electronic components in their small internal space, which increases the computing load under the conditions of system miniaturization, and the method of designing an appropriate heat dissipation mechanism will affect the stability and efficiency of the device. To solve the aforementioned problem, the purpose of this study was to optimize the design of the cooling system in the T/R modules of communications systems by integrating heat pipes, cooling fans, cooling fins, and cooling chips within a limited space. In addition, based on the different directional clamp-in configuration methods of heat pipes within copper panels, we designed four types of cold plates and utilized the finite element method (FEM) to simulate and analyze the heat dissipation performance of all cold plates. The simulation results reveal that type I and II cold plates can achieve a better heat dissipation performance. Finally, these types (I and II) were selected for production and experimental verification. The results show that heat dissipation performances were similar to simulation results. The results also verify that type II has a better temperature uniformity and heat transfer efficiency. This is evident that the cooling mechanism described in this study is viable for practical applications. The proposed mechanisms can also provide a reference for heat dissipation design patterns in different electronic module settings. In addition, the same products with narrow, closed, and non-convective internal space features include defense weapon system millimeter-wave radar, missile system guidance, control section core computing unit, 5G communication system, high-speed computing workstation/server, etc. Through the active heat dissipation configuration of the structure of this experiment, the relevant adaptive design is carried out to achieve the temperature range control and meet the heat dissipation requirements of the system.

2. Description of Heat Dissipation System Structure and Issues

2.1. Heat Dissipation System Structure Design

This study optimized the configuration design of cooling modules based on an internal clamp-type cold plate for the T/R modules of high-power 5G communication devices. The device has 32 sets of T/R modules, and the power consumption reached 1.54 KW. The research took a single module to optimize the configuration design of the heat dissipation module. The system primarily consists of a T/R module, control module, power supply module, and casing with system structure as shown in Figure 1. The T/R module generates massive amounts of thermal energy during operation and requires a heat dissipation module for suitable cooling to ensure that the system does not fail due to excessive temperatures. To achieve a better heat dissipation performance, this study integrated the design of the T/R module and heat dissipation modules and proposed a heat dissipation module that could be applied to 5G communication systems. The integrated heat dissipation module consists of components such as heat pipes, internal clamp-type cold plate, thermoelectric cooling chip (TEC), and cooling fans that form an active heat dissipation system as shown in Figure 2. The general heat transfer structure came from contact with the 48 W power T/R module by the lower cold plate. The heat pipe transfers thermal energy from the lower cold plate to the upper cold plate where the TEC, cooling fins, and fans expel thermal energy outside the system. The general heat transfer path was as shown in Figure 3. The

heat dissipation performance of the thermoelectric cooling chip and fan can be controlled by adjusting the input current. Accordingly, the heat dissipation module proposed by this paper is an active heat dissipation mechanism.

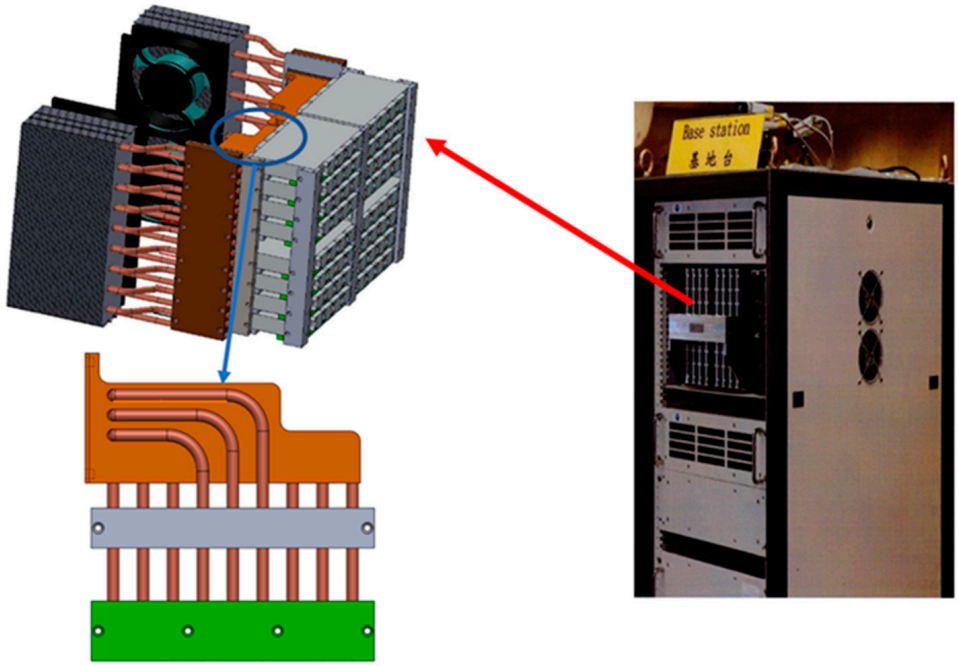

Figure 1. 5G Communication System Structure and Heat Dissipation Module Configuration.

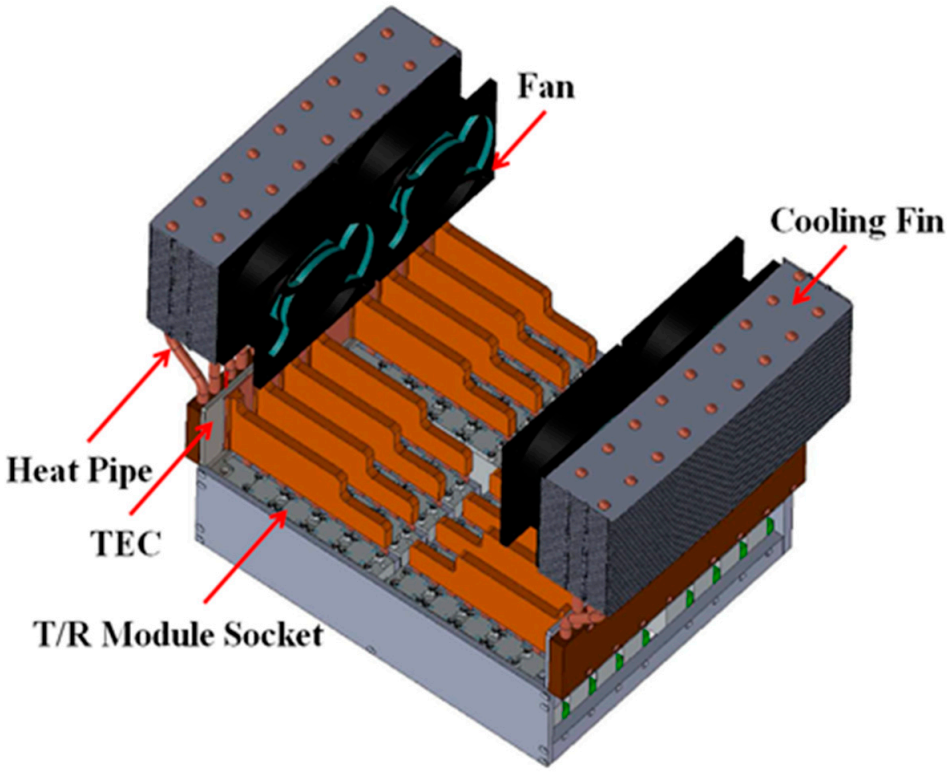

Figure 2. Integrated T/R Module and Heat Dissipation Module.

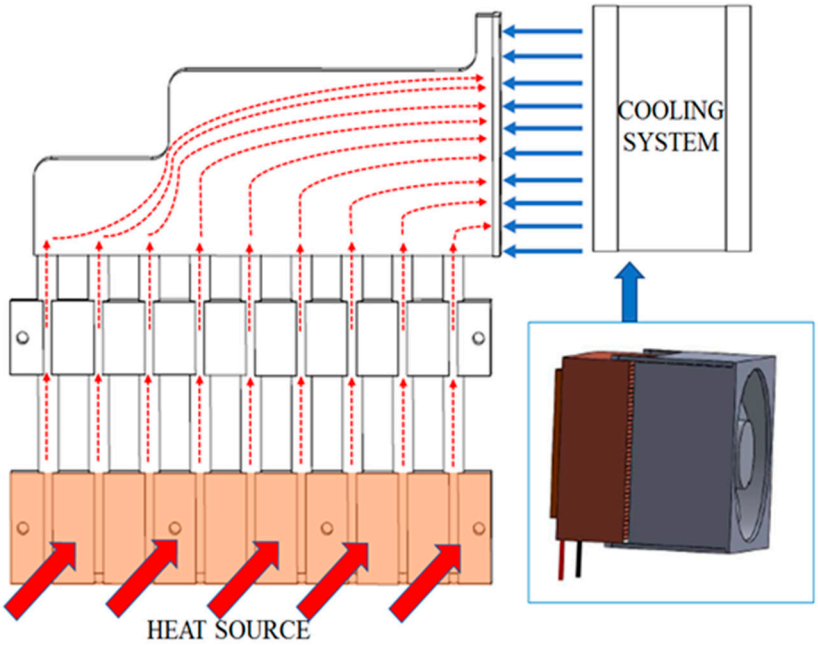

Figure 3. The Thermal Energy Transfer Path.

2.2. Description of Issues

The aforementioned 5G communication system's general structure is limited by factors such as size and configuration layout of electronic components, limiting the size and shape of thermal components. The size and shape of the heat dissipation module in Figure 2 are limited to the system's space resulting in heat dissipation mechanisms restricted by conditions. Considering the limitations to size, appearance, design and manufacture, the vapor chamber is challenging and costlier. Based on this fact, this study focused on the upper and lower cold plate by utilizing an internal clamp-type cold plate design. Moreover, the heat dissipation module designed by this study shows that due to the size limitations of the lower cold plate and heat pipe, it was not possible to improve the design and heat dissipation performance through configurations. Therefore, the deciding factor and key issue for the performance of this study's heat dissipation module was determined by improving the configuration design for a better thermal equalization in the upper cold plate. The purpose of this study was to achieve a better heat dissipation performance through different design configurations of internal clamp-type cold plates.

3. Internal Clamp Cold Plate Design

This study utilized nine heat pipes clamped internally to the upper and lower copper panels, forming the internal clamp cold plate structure. A better thermal equalization was achieved in the upper cold plate to improve the cooling performance of the heat dissipation system. Based on the arrangement method of internal heat pipes on the copper panel, we designed four types of cold plates. The lower copper panel's heat pipes and clamping arrangement method were identical. Details of all cold plates are as below.

1. Type I: Heat pipes 4 to 6 were curved and clamped internally to the upper copper panel, the inner and outer diameters of each curved pipe were 15 mm and 21 mm, respectively; heat pipes 1, 3, 7, 8, and 9 were straight and each pipe had a length of 99 mm as shown in Figure 4.
2. Type II: Heat pipes 10 to 12 were curved and clamped internally to the upper copper panel, and the inner and outer diameters of each curved pipe were 10 mm and 21 mm, respectively; heat pipes 1 to 9 were straight, and each pipe had a length of 94 mm as shown in Figure 5.

3. Type III: Heat pipes 1 to 6 were straight and clamped internally to the upper copper panel, and each pipe had a length of 120 mm; heat pipes 7, 8, and 9 were straight and 99 mm in length as shown in Figure 6.
4. Type IV: Heat pipes 1 to 9 were straight with lengths of 94 mm as shown in Figure 7.

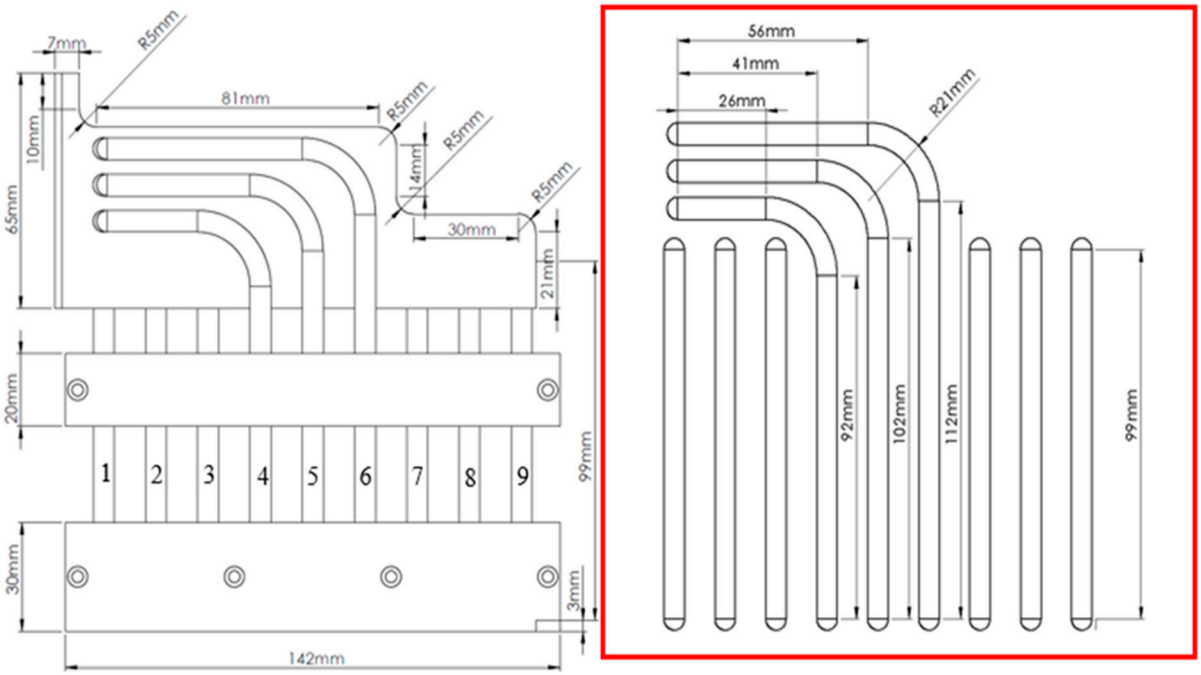

Figure 4. Configuration of Type I cold plate.

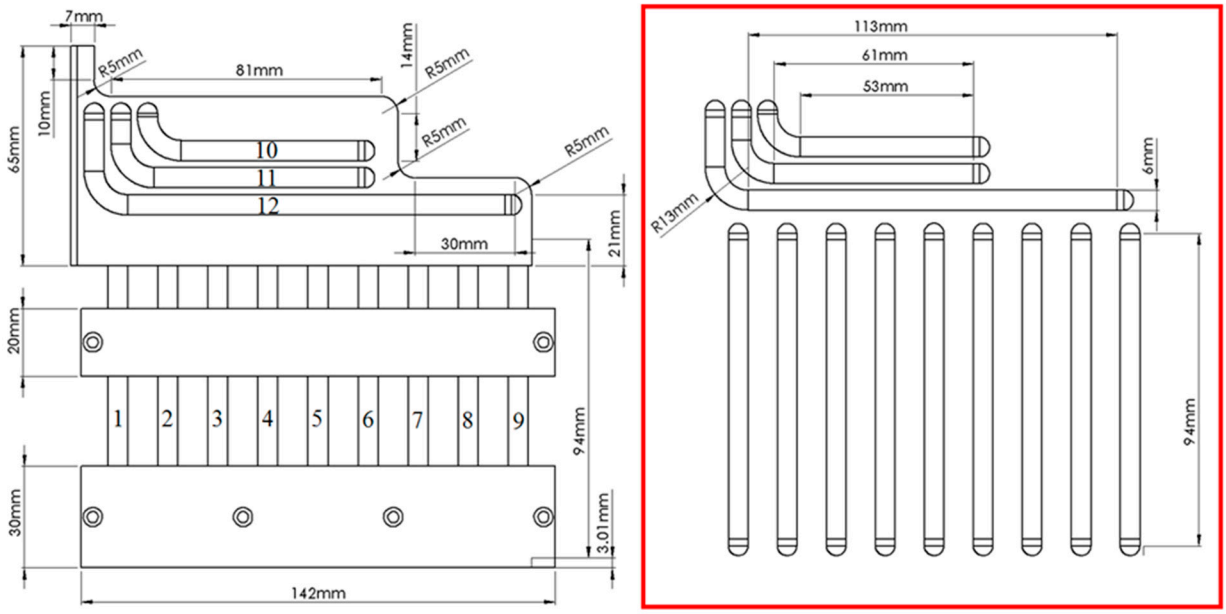

Figure 5. Configuration of Type II cold plate.

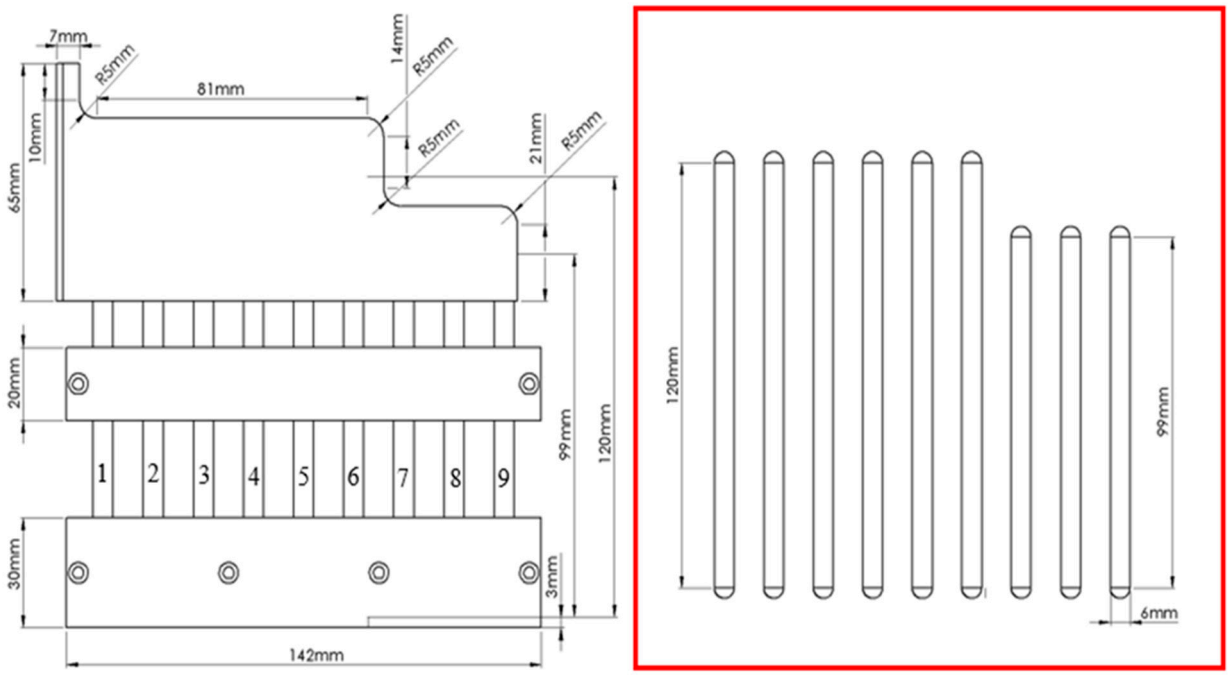

Figure 6. Configuration of Type III cold plate.

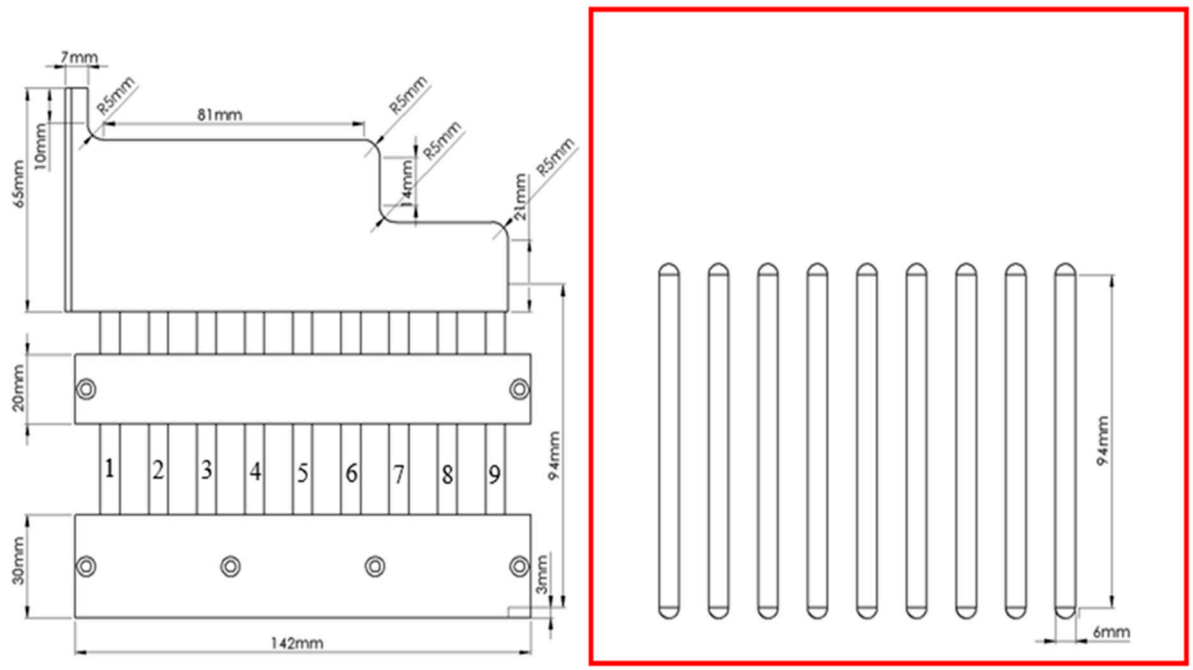

Figure 7. Configuration of Type IV cold plate.

4. Heat Dissipation Performance Simulation and Analysis

This study utilized the FEM to conduct simulation analysis of the heat dissipation performance for each cold plate configuration. Each configuration's temperature change data and stable temperature differences were observed for analyzing heat transfer flow direction and dissipation efficiency before using the results to explore which configuration achieved better cooling performance. This avoided having to construct equipment for measurement and testing, reducing costs and shortening research and development time. Detailed explanations of simulations are given below.

4.1. Simulation System Design

The data simulation process of this study first required the use of a graphics editor to draw and design different cold plate configurations and use the FEM simulation software to design cold plate grids and set parameters such as material characteristics, environment temperature, and boundary conditions (including heat transfer efficiency formed by cooling fans, cooling fins, and thermoelectric cooling chips).

The lower cold plate of the general heat dissipation system is heated by a 48 W fixed heat source (simulating the heat source generated from the operation of a single T/R Module). Heat travels up the heat pipes to the upper cold plate to perform thermal convection, besides heat dissipation through natural convection and the heat expelled by the TEC attached at the cooling end.

The critical components encompassed in simulation analysis include the upper/middle/lower heat-transfer panels, heat pipes, and cooling system. Heat pipes 9 to 12 utilized their fast thermal equalization and super thermal conductivity to transfer the massive amount of heat generated by the T/R module to the active cooling system to quickly expel heat. Using different heat pipe configuration designs in the limited space of the upper heat transfer panel, 3D models were utilized to conduct data simulations with the finite element method. Stable state analysis was used to differentiate the heat dissipation benefits of different heat pipe configurations.

4.2. Simulation Parameter Settings

4.2.1. Material Selection

The metallic components used in this study were the upper/middle/lower plates and the straight/curved heat pipes. Consideration of the null end of heat pipes and the physical characteristics of all materials are as shown in Table 1. The three types of materials utilized in this study include aluminum (6061-T4), red copper (C1100), and oxygen-free (C1020).

Table 1. Material and Physical Parameters.

Item	Element	Spec. Heat C_p	Density ρ	Thermal Conductivity k
		$J/(kg \times K)$	kg/m^3	$W/(m \times K)$
a	Upper Heat Transfer Panel (Copper C1100)	386	8940	391.1
b	Middle Heat Transfer Panel (Aluminum 6061-T4)	872	2700	247
c	Lower Heat Transfer Panel (Copper C1100)	386	8940	391.1
d	Direct Heat Pipe (Oxygen-free copper C1020)	385	8940	20,000
e	Curved Heat Pipe (Oxygen-free copper C1020)	385	8940	16,000

4.2.2. Physical Model

The governing equation used in the simulation of heat dissipation components in this study was primarily based on thermal conductivity Equations (1)–(5). Generally, heat transfer was divided into heat conduction, heat convection, and heat radiation, although the simulations and analysis of results in this study did not consider heat radiation conditions. During experimentation, one side of the lower cold plate was attached to a heat generator (heat source) while the other end of the lower cold plate was attached to thermal insulation cotton to insulate against heat; therefore, the boundary condition was set as the heat insulation boundary while the remaining surface area was in direct contact with environmental air, which was set as the natural convection boundary. Generally, the heat transfer coefficient of air medium under natural convection was 5–25 $W/m^2 \cdot K$.

The natural convection coefficient set in this study was 20 $W/m^2 \cdot K$, and environmental temperature was set as T_0 = 25 °C.

$$k \equiv -\hat{q}/\frac{\partial T}{\partial X} \tag{1}$$

$$Q_{conduction} = kA\frac{\Delta T}{L} \tag{2}$$

$$R_{th} = \Delta T/Q \tag{3}$$

$$\hat{q} = Q/A = k\Delta T/L \tag{4}$$

$$\rho C_P \frac{\partial T}{\partial t} + \nabla \cdot (-k\nabla T) = Q \tag{5}$$

4.3. Simulation Result Analysis

This study utilized multiphysics simulation and analysis software (COMSOL) coupled with FEM to verify the heat dissipation performance of the four configurations established in the simulations of this study. Based on the simulation results, the maximum and minimum temperatures of each configuration are as shown in Table 2. Surface temperature simulations were as shown in Figures 8–11; these results show that when the heat dissipation structure system achieved stability, the maximum surface temperature of type I is 90.1 °C while the minimum temperature is 87.2 °C. Curved heat pipes 4 to 6 quickly transferred heat to the cold end while the straight heat pipes 7 to 9 located far from the cold end exhibited higher temperatures compared with other areas; the isothermal contour was as shown in Figure 8. The maximum surface temperature in type II was 88.6 °C while the minimum temperature was 85.9 °C. The results show that the thermal transfer of this configuration achieves good thermal equalization; the surface temperature is as shown in Figure 9. The maximum surface temperature in type III was 94.2 °C while the minimum temperature was 90.9 °C. The temperature gradient distribution trend is downward when close to the cold end; the surface temperature is as shown in Figure 10. The maximum surface temperature in type IV was 94.5 °C while the minimum temperature was 90.5 °C. The temperature gradient distribution trend was downward when close to the cold end; the surface temperature was as shown in Figure 11. Based on known configurations, both types III and IV displayed similar temperature distribution trends.

Table 2. A Comparison of High and Low Temperature Simulations.

	Type I	**Type II**	**Type III**	**Type IV**
Max Temperature	90.1 °C	88.6 °C	94.2 °C	94.5 °C
Min Temperature	87.2 °C	85.9 °C	90.9 °C	90.5 °C

Based on the simulation results, the heat dissipation effects of type II were found to be superior to other types and also displays good thermal equalization, and can be referenced for the future design of other configurations. During simulations, this study did not include any forced convections to observe the differences in heat dissipation performance between each configuration. In practical applications, TECs, cooling fins, and cooling fans can be used in combination to improve heat dissipation efficiency and achieve the purpose of controlling system temperature.

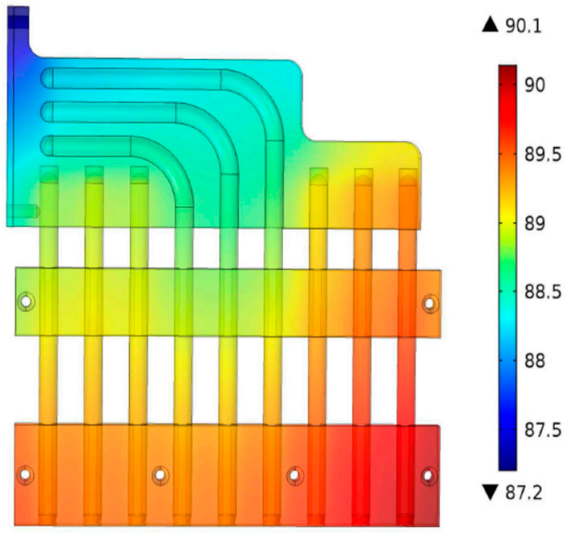

Figure 8. Temperature profile (Type I).

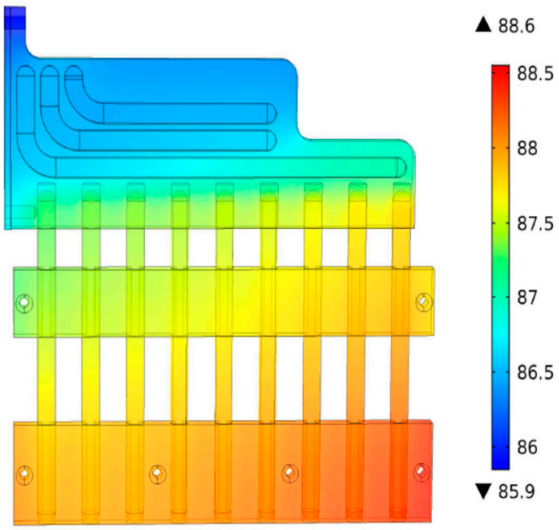

Figure 9. Temperature profile (Type II).

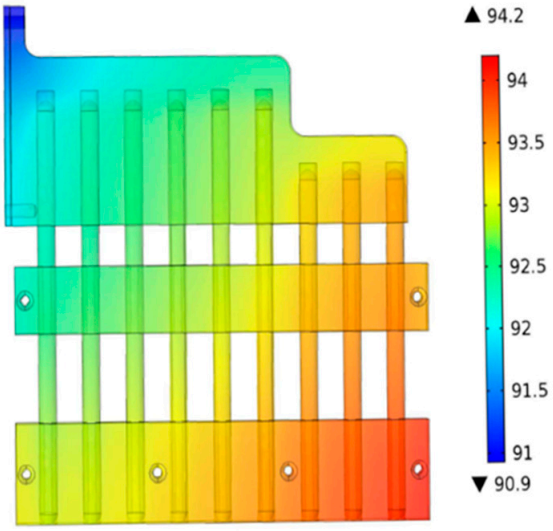

Figure 10. Temperature profile (Type III).

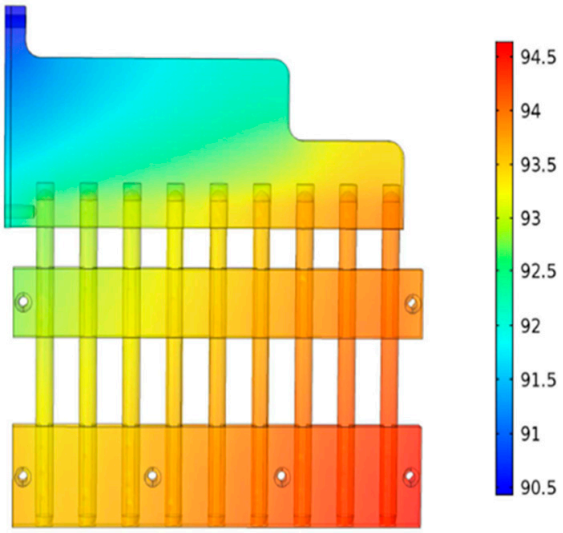

Figure 11. Temperature profile (Type IV).

5. Experiment Verification

Based on the simulation results, the superior types I and II were selected for test production and integration with hardware configurations that include heat pipes, cooling fans, cooling fins, TECs, and sensors. The implemented general experimental structures were classified into four major systems: computer system, measurement system, power supply, and cooling system. The purpose of the experiment was to replace an actual T/R module with a heat generator that supplies a stable heat source to test the temperatures on the surface of the test system as well as the internal measuring point of the heat source. The temperature changes in the system's passive and active heat dissipation mechanisms were observed to verify whether the simulation result trends were identical and the heat dissipation performance when an active cooling system was added. This confirmed whether the heat dissipation type designed in this study could meet heat dissipation performance requirements.

5.1. Experiment Equipment

The experimental design of this study utilized a K-type thermocouple connected to the surface of the test system and heat generator (heat source) with measuring points distributed at four points on the upper panel, four points each on the lower panel, and within the heat generator. The points were connected to the temperature data capture component for real-time measurement of temperature data. Plans of the active heat dissipation system are as shown in Figure 12. Hardware specifications were as mentioned in Table 3. Details of the four major hardware systems in this study are as follows:

Table 3. Specifications of the hardware.

Item	Hardware	Manufacturer	Type Specification
1	IPC-610-H	ADVANTECH	Industrial Computer P4–2.4 GHz, 2 G RAM
2	NI cDAQ-9178	National Instruments	High performance data streams:7, Timing resolution:12.5 ns
3	NI 9212	National Instruments	8 channels, 2 internal cold-junction compensation channels
4	Thermocouple	Thermocouple Technology	K-Type
5	Power Supply	Topward 6303 A	DC 30 V, 3 A
6	Power Supply	Gwinstek SPS-1820	DC 18 V,20 A
7	Thermo Electric Cooler	KRYOTHERM Drift-0.6	V_{max} = 24.6 V, I_{max} = 15.1 A, Q_{max} = 229.3 Watt
8	FAN	Symbang D17251V24HB	DC 24 V, 0.87 A, 3400 RPM

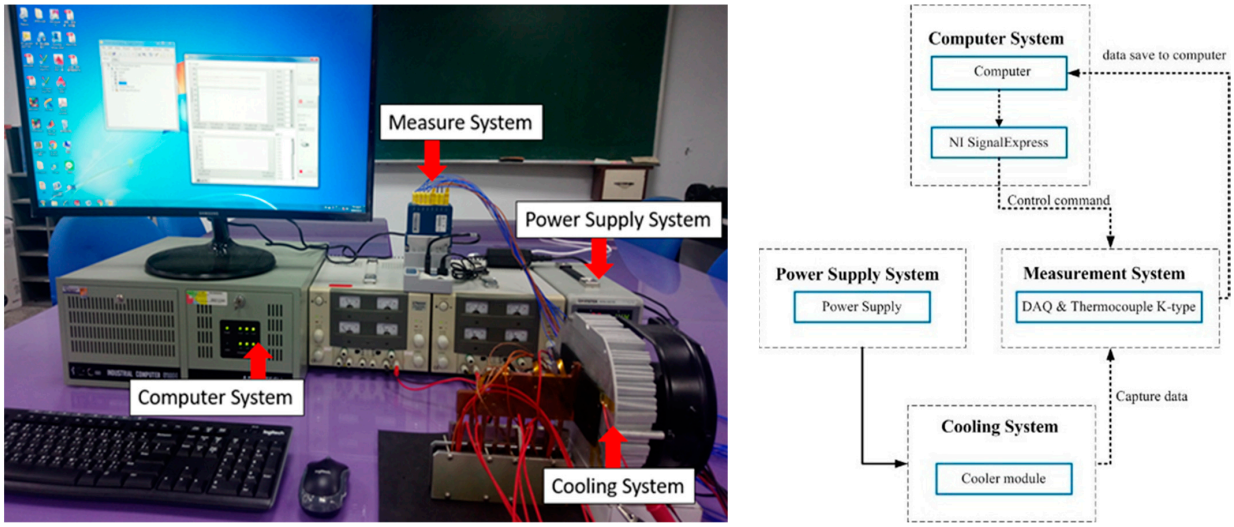

Figure 12. A schematic of system planning for the active heat dissipation device.

5.1.1. The Computer System:

1. One computer equipped with Signal Express Software to compute the captured signal.
2. Signal capture software:

Software, in combination with the data capture system designed by National instruments, provides real-time record and capture of signals generated by the system. Settings can be adjusted for capture speed, temperature range, capture time, sensor type, cold point compensation method, capture channel, and record format.

5.1.2. The Measurement System:

1. The system uses the DAQ data measure interface which captures, processes, and converts the signal source from the sensor (thermocouple). It primarily consists of a high-performance measurement and controller card, signal processing module, filter amplifier, and charge amplifier. Combined with Signal Express included in the graphic control software, temperature data captured by the measurement system records complete data in real time.
2. Actual testing was conducted on types I and II as they performed as the top candidates in the simulation as shown in Figures 13 and 14.

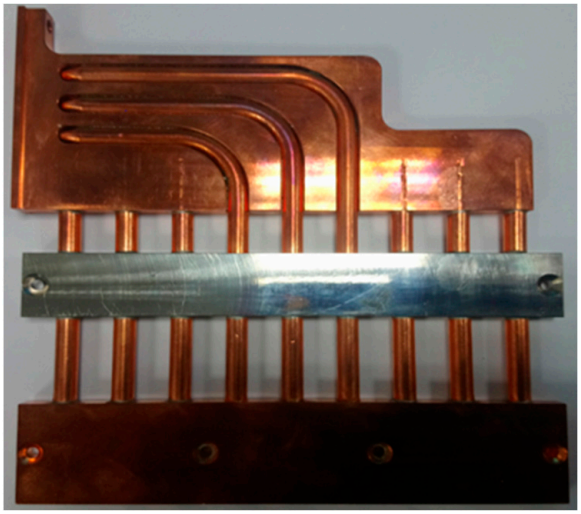

Figure 13. Specimen Type I.

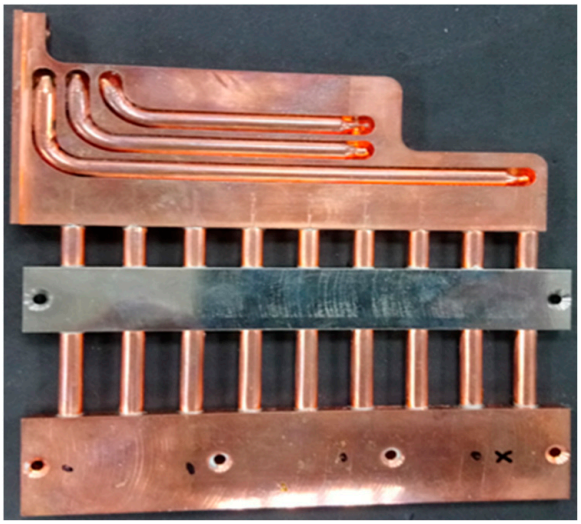

Figure 14. Specimen Type II.

3. The temperature data measure device has 8 channels and can simultaneously capture 8 sets of temperature data and is designed with 2 sets of compensation for internal cold points.
4. During testing, this study used K type×8 thermocouples performing synchronized data capture at 12 ms for each data item. Measurements of the upper panel and internal heat generator were conducted as shown in Figures 15 and 16.

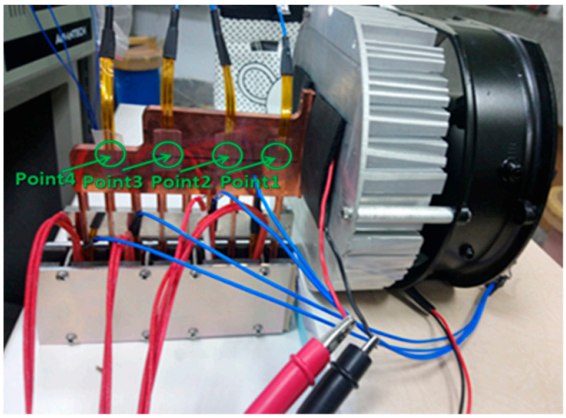

Figure 15. Measurement configuration diagram.

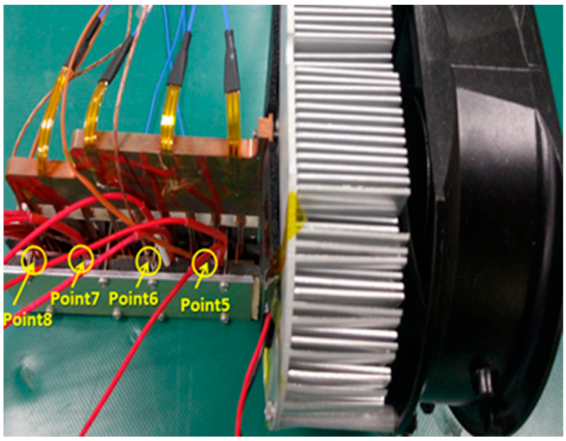

Figure 16. Measurement configuration diagram.

5.1.3. The Power Supply System:

1. This study utilizes three power supplies to provide the power required by standard heat source generators; supply to the cooling fan and thermoelectric cooling chip is as shown in Figure 17, and heat generator is as shown in Figure 18.

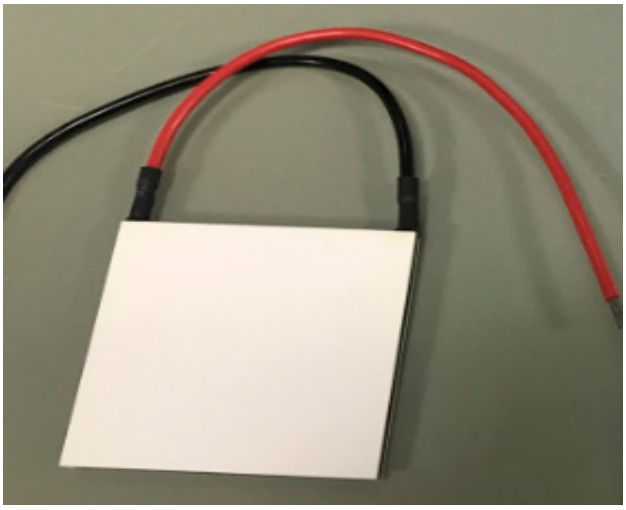

Figure 17. A thermoelectric cooling chip (TEC).

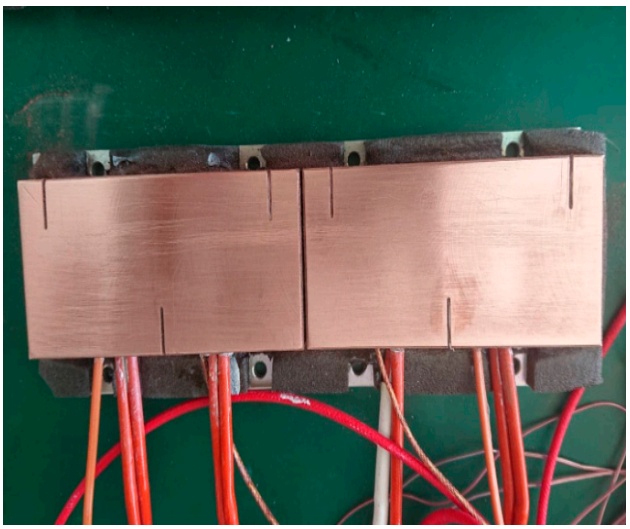

Figure 18. A heat generator (Dummy Heater).

2. Power supply conditions, cooling fan 23 VDC/0.9 A, thermoelectric cooling chip 15.3 VDC/4.51 A, and heat generator 20 VDC/2.4 A.

5.1.4. The Cooling System:

The heat pipes, high-performance thermoelectric cooling chips (maximum cooling power can reach 229.3 W), cooling fins, and fans were used to construct the heat dissipation system as shown in Figure 19.

5.2. Discussion

This study conducted experiments to verify type I and II passive heat dissipation systems from simulation results to determine whether their temperature distribution trend was identical and to confirm the cooling performance of the designed types of heat dissipation system. However, under conditions of passive heat dissipation, temperature control could not achieve the –20 °C~+70 °C temperature range required by standard

electronic components. This study maintained a stable-state temperature above 70 °C in both simulation and test results, so an active cooling system was required. This study also utilized TECs to quickly absorb heat and used cooling fins and fans to transfer heat outside the system. Hopefully, the test verifies the heat dissipation performance of types I and II passive heat dissipation systems and their compliance with the heat dissipation requirements of the system.

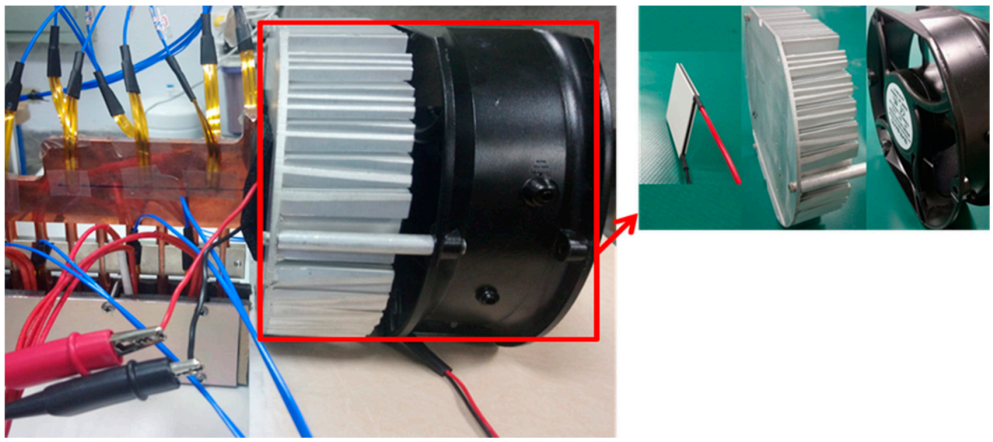

Figure 19. A heat dissipation system.

The experiment first uses a 48 W heat generator to heat the system for 3600 s for both types I and II under conditions where active cooling systems are solely reliant on passive heat dissipation to simulate the heat generated from the T/R module and observe changes in temperature. Next, the active cooling system was activated for 1800 s simultaneously observing the cooling curve before shutting off the 48 W heat generator and continuing operation of the cooling system for 1800 s, and cooling the system to a stable state. Measurement data of upper panel temperatures for both types are mentioned in Table 4. Results show that during the 3600 s period without the active heat dissipation system, type I achieved a maximum temperature of approximately 83.5 °C, which is higher compared with the 79.2 °C of type II; in addition, the temperature difference between the four measurement points of both types revealed a better thermal equalization by type II. This trend remains uniform after the active cooling system is activated and temperatures enter a stable state. In terms of temperature control, temperatures of type I were approximately 46.1–50.6 °C, and that of type II was approximately 43.4–45.8 °C, indicating a superior performance of type II in heat dissipation. Additionally, when the heat generator was stopped after 5400 s, the temperature curve of the figure clearly shows a faster cooling of type II and entered a steady state when compared with type I. This comparison shows that the heat dissipation performance of type II is superior to that of type I as shown in Figures 20 and 21. Measurement data from the temperatures in the two types of heat generators (as in Table 5) show that during the 3600 s period without active heat dissipation, both types I and II measured at above 90 °C, which is more than the 70 °C required for temperature control. After the active cooling system performed temperature control for 1800 s, the temperature evidently decreased to 54~57 °C and met the cooling requirements of the system as shown in Figures 22 and 23.

Table 4. The comparison of upper-plate measures.

	Type I				Type II			
Temperature	**Point 1**	**Point 2**	**Point 3**	**Point 4**	**Point 1**	**Point 2**	**Point 3**	**Point 4**
No active cooling which in 3600 s	79.6 °C	72.0 °C	81.7 °C	83.5 °C	76.5 °C	76.3 °C	79.2 °C	75.3 °C
Active cooling which in 5400 s	47.2 °C	46.1 °C	49.6 °C	50.6 °C	43.8 °C	44.2 °C	45.8 °C	43.4 °C

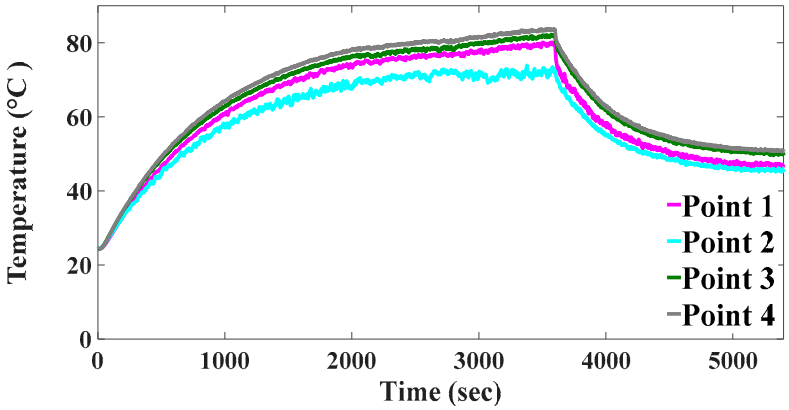

Figure 20. Temperature responses in Type I upper-plate point.

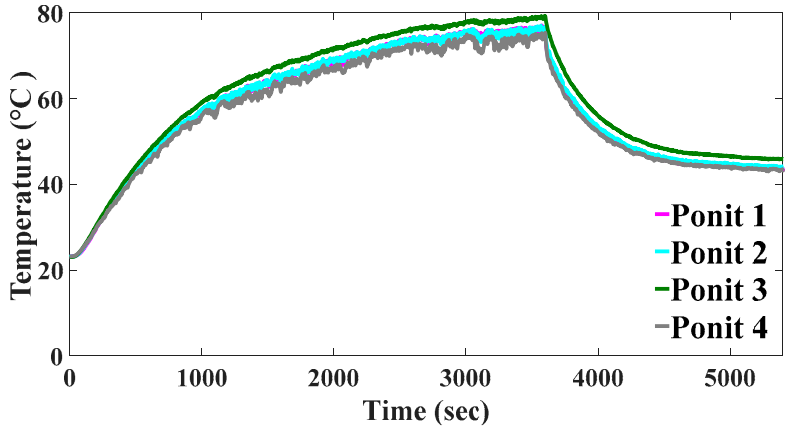

Figure 21. Temperature responses in Type II upper-plate point.

Table 5. A comparison of heating source measurement.

	Type I				Type II			
Temperature	**Point 5**	**Point 6**	**Point 7**	**Point 8**	**Point 5**	**Point 6**	**Point 7**	**Point 8**
No active cooling which in 3600 s	90.1 °C	89.4 °C	91.3 °C	90.9 °C	90.2 °C	88.3 °C	90.2 °C	89.6 °C
Active cooling which in 5400 s	56.2 °C	55.7 °C	57.7 °C	57.4 °C	55.1 °C	54.0 °C	56.0 °C	55.4 °C

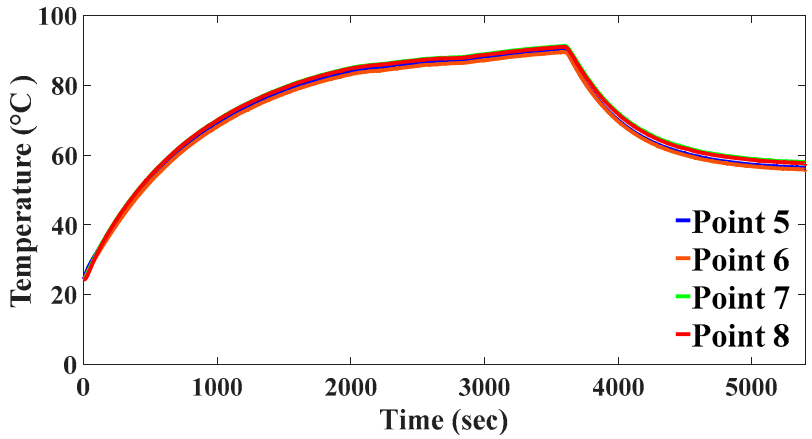

Figure 22. Temperature responses in Type I heat-source point.

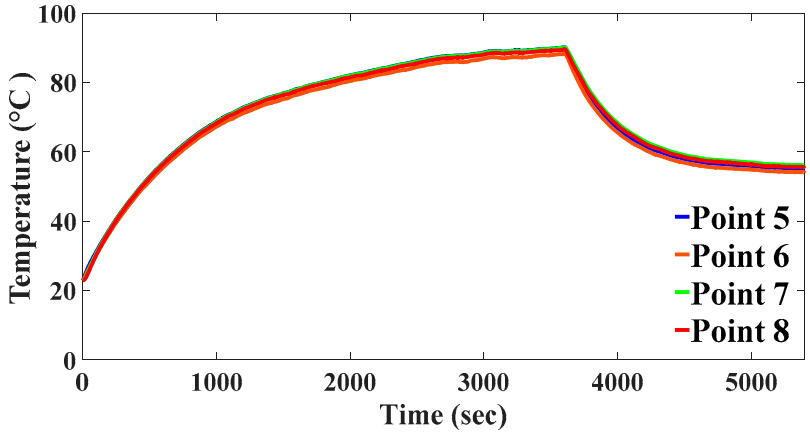

Figure 23. Temperature responses in Type II heat-source point.

When the system was heated with the 48 W heat generator at environment temperature and the active cooling system was activated for 3600 s before measurement, the observed temperature data of the upper panel for both types was as shown in Figures 24 and 25. Data at 3600 s, once the stable state is entered, is as shown in Table 6. Results show that the maximum temperature of type I was approximately 50 °C, which is higher than the maximum temperature of 44.4 °C for type II. When measuring the temperature differences of the 4 points in both types, type II performed better in thermal equalization as is evident by the increase in the temperature curve and that type II entered the stable state at a faster rate. Based on the heat source temperature measurements of both types (Figures 26 and 27) and comparing data at 3600 s after entering the steady state (Table 7), the results showed that the maximum temperature of type I heat source was 57.2 °C while that of type II was 54.9 °C. Based on these results, the heat dissipation efficiency of type II is superior to that of type I and complies with the heat dissipation requirements of the system.

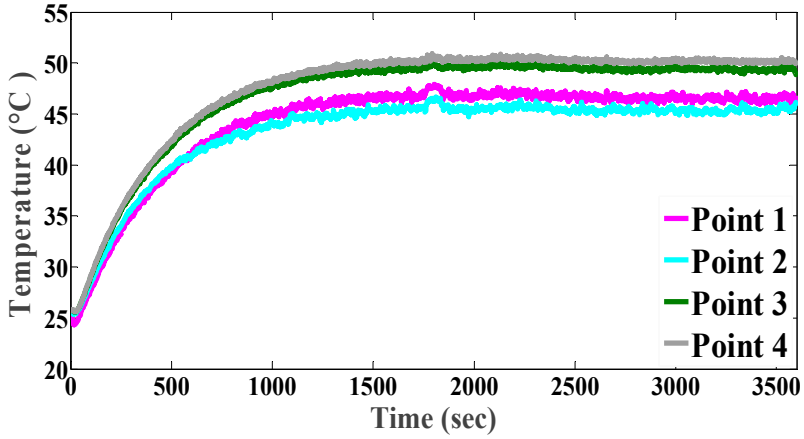

Figure 24. Temperature responses in Type I upper-plate point.

Table 6. Upper-plate experiment comparison.

	Type I				Type II			
Temperature	**Point 1**	**Point 2**	**Point 3**	**Point 4**	**Point 1**	**Point 2**	**Point 3**	**Point 4**
Active cooling which in 3600 s	46.7 °C	46.2 °C	48.7 °C	50.0 °C	42.2 °C	42.7 °C	44.4°C	41.9 °C

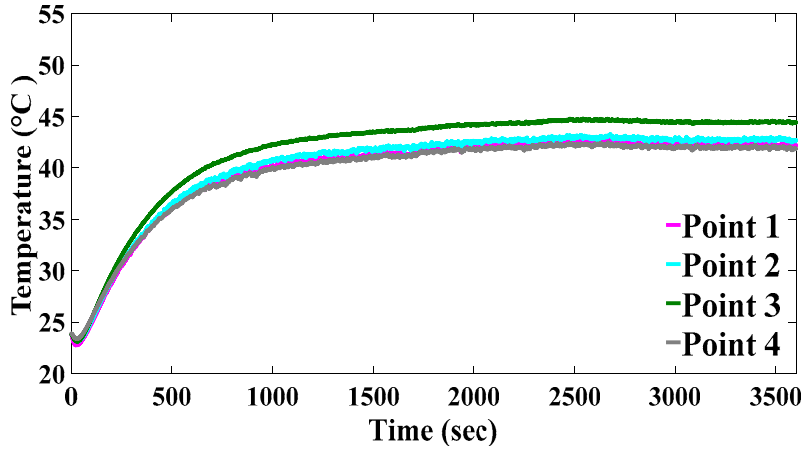

Figure 25. Temperature responses in Type II Upper-plate point.

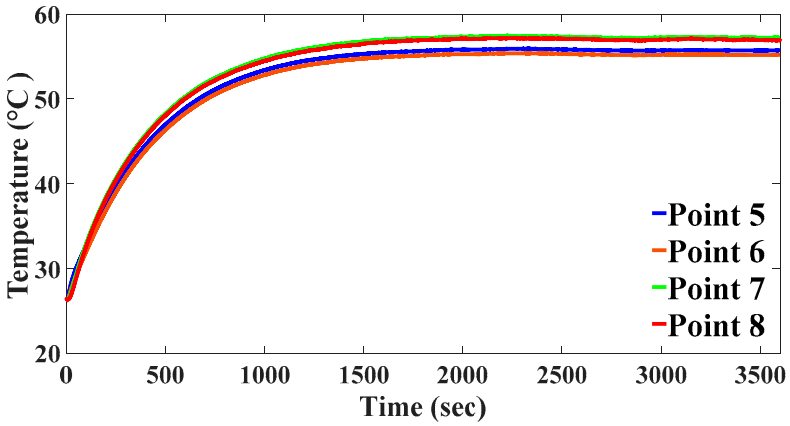

Figure 26. Type I heat-source temperature.

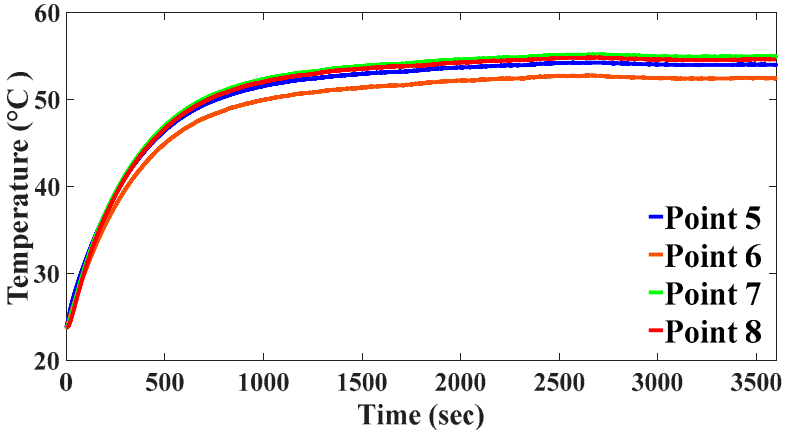

Figure 27. Type II heat-source temperature.

Table 7. Heating source experiment comparison.

	Type I				Type II			
Temperature	**Point 5**	**Point 6**	**Point 7**	**Point 8**	**Point 5**	**Point 6**	**Point 7**	**Point 8**
Active cooling which in 3600 s	55.7 °C	55.2 °C	57.2 °C	56.9 °C	54.0 °C	52.4 °C	54.9 °C	54.6 °C

The four points temperature average response curves on the bottom dummy heater of the two configurations were measured, and they were Type I HS(I) and Type II HS (II) respectively, and the temperature curve of the cold surface of the TEC in contact with the upper heat transfer plate was as shown in Figure 28. Type I Cold (I) and Type II Cold (II) were calculated by the thermal resistance formula R = (T2 − T1)/P, while Type I and II were calculated to obtain TR-1 and TR-2, respectively. According to the thermal resistance response curve (Figure 29), the thermal resistance value of Type II was 0.73 °C/W, lower than Type I thermal resistance value of 0.88 °C/W, which has better heat dissipation performance, and the cooling chip starts in the thermal resistance analysis. The startup takes a short period of time to cause the transient response of the cold surface temperature to drop rapidly.

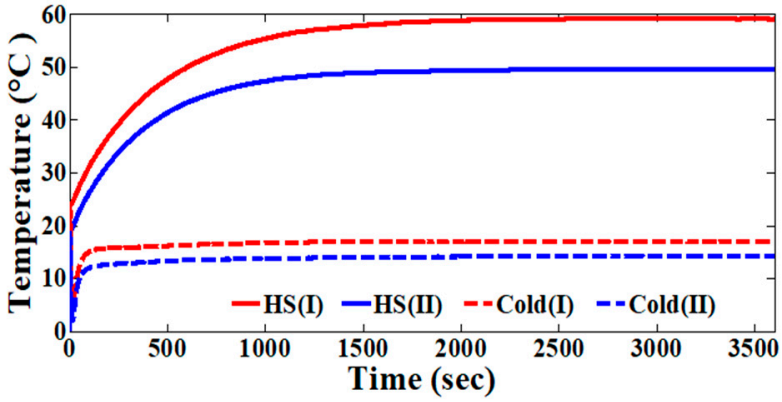

Figure 28. Dummy Heater and cold surface of the TEC temperature response.

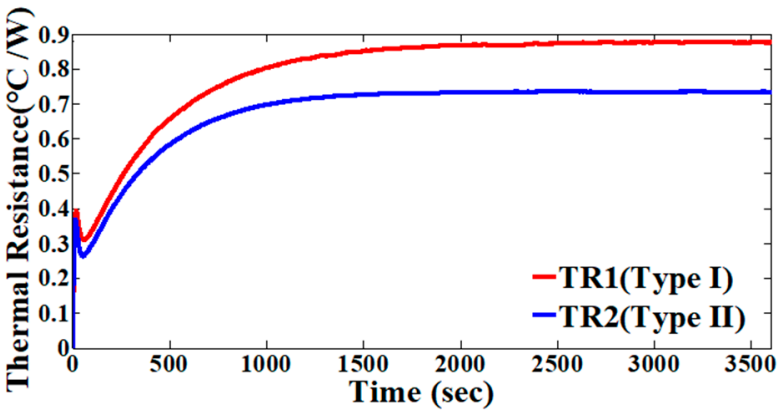

Figure 29. Thermal Resistance.

6. Conclusions

In this study, we designed a high-performance heat dissipation module for 5G communication systems. Most active cooling systems are mainly designed with a combination of components such as fans, vapor coolers, or liquid coolers. They are not properly integrated with heat-source components, and weight and space constraints are not considered, so they cannot be configured in a small space. In this work, the heat dissipation elements and the heat source elements are integrated, and the system's space limitation is considered so that the proposed heat dissipation mechanism can be applied to a small space and meet performance requirements. The system integrates heat pipes, cooling fans, cooling fins, and thermoelectric cooling chips in limited space conditions in order to optimize heat dissipation design for T/R modules. Cold plates designed with the FEM were simulated and analyzed for heat dissipation performance before using the simulation results to conduct production and experiments for verification. Out of the proposed four types of heat dissipation mechanisms, simulation results showed superior heat dissipation performance of types

I and II. During the simulation stage, initial conditions, boundary condition settings, errors in model construction, and wear to the heat transfer efficiency of heat pipes when curved may have led to differences in simulation results and testing of actual systems. In addition, there is also a systematic error (including measurement error and capture Interference) and a random error in the experiment, where the measurement error is based on the Type K Thermocouples coefficients, which is determined according to NIST ITS-90 specification, converted to temperature. The resulting error range is ±0.05 °C in 0 °C to 500 °C, and the error rate is 0.01%, while Capture Interference is a temperature data extractor (Ni-9212) in using K type thermocouples precision to 0.01 °C. This part will also cause the difference between simulation data and experimental data. The comparison between the test results and the numerical simulation results shows that the trend between the experimental and simulation data is consistent. Some errors still exist. The maximum error of the steady-state temperature at the contact point of the heat source (Point 5~8) is 1.8%; however, the initial heat dissipation properties of the designed mechanisms could still be observed to provide a reference for future designs of active heat dissipation mechanisms. Subsequent experimental results in this study show that heat dissipation performances were similar to simulation results. Without the active heat dissipation system, type I achieved a maximum temperature of approximately 83.5 °C, which is higher compared with the 79.2 °C of type II; in addition, the temperature difference between the four measurement points of both types revealed a better thermal equalization by type II. The active cooling system was activated. Once the stable state is entered, the maximum temperature of type I was approximately 50 °C, which is higher than the maximum temperature of 44.4 °C for type II. It is evident by the increase in the temperature curve that type II entered the stable state at a faster rate. Based on these results, the heat dissipation efficiency of type II is superior to that of type I. From the different design concepts of types I and II, the heat conduction directivity of the heat pipe was found to be a key factor, so that the overall system quickly converged to a steady state. Besides, through the heat pipe embedded in the upper end of the heat transfer plate design difference, type II optimized design exhibited a better uniform temperature effect, clearly suggesting that the heat dissipation configurations depicted in this study are viable in practical applications. The components (TEC, heat pipe, fin) used in the active heat dissipation mechanism proposed in this work are all widely used products, which have the advantages of mature production technology and low cost. In addition, the two clamp-in cold plates designed by this paper are composed of heat pipes and copper plates. Compared with the 3D vapor chamber, the manufacturing process is simpler and the cost is lower. The simulation and experimental results show that the heat dissipation performance of the heat dissipation mechanism proposed in this work can meet the specification requirements, so it can achieve the purpose of reducing costs and meeting performance requirements. In the future, the results of this study could be used in combination with relevant control theories while designing temperature control systems for achieving energy conservation, low cost, and highly efficient temperature control performance. This can be applied to other high-power electronic products to ensure that they may perform at their intended levels.

Author Contributions: Conceptualization, T.-P.Y. and Y.-L.L.; Formal analysis, T.-P.Y. and Y.-L.L.; Investigation, Methodology, T.-P.Y. and Y.-L.L.; Resources, T.-P.Y.; Validation, T.-P.Y.; Review & editing, Y.-L.L., Y.-W.L. and S.-W.M. All authors have read and agreed to the published version of the manuscript.

Funding: This research received no external funding.

Institutional Review Board Statement: Not applicable.

Informed Consent Statement: Not applicable.

Data Availability Statement: The datasets used and analyzed during the current study are available from the corresponding author on request.

Conflicts of Interest: The author declares no conflict of interest.

Abbreviations

CPU	central processing unit
VC	vapor chambers
AR	aspect ratio
TEC	Thermo Electric Cooler

Nomenclature

A	Cross-sectional area perpendicular to heat transfer direction
C_P	specific heat capacity
h	natural convection coefficient
ΔT	Temperature difference of heat passing section
T_0	environmental temperature
T	Temperature
k	thermal conductivity of material
ρ	density of the material
$\hat{q}$	heat flux
t	time
L	Heat transfer path length
$\frac{\partial T}{\partial X}$	Temperature gradient
Q	heat generation
$Q_{conduction}$	Thermal conductivity

References

1. Azar, K.; Mandrone, C.D. Effect of Pin Fin Density of the Thermal Performance of Unshrouded Pin Fin Heat Sinks. *J. Electron. Packag.* **1994**, *116*, 306–309. [CrossRef]
2. Lehmann, G.L.; Wirtz, R.A. Convection from Surface Mounted Repeating Ribs in a Channel Flow. In Proceedings of the American Society of Mechanical Engineers, Winter Annual Meeting, New Orleans, LA, USA, 9–14 December 1984. ASME Paper No.84-WA/HT-88.
3. Lehmann, G.L.; Wirtz, R.A. The Effect of Variations in Stream-Wise Spacing and Length on Convection from Surface Mounted Retangular Components. *Trans. ASME* **1985**, *111*, 39–47.
4. Arvizu, D.E. Experimental Heat Transfer from an Array of Heated Cubical Elements on an Adiabatic Channel Wall. Ph.D. Thesis, Department of Mechanical Engineering, Stanford University, Stanford, CA, USA, 1981.
5. Lin, S.-C.; Chuang, F.-S.; Chou, C.-A. Experimental study of the heat sink assembly with oblique straight fins. *Exp. Therm. Fluid Sci.* **2005**, *29*, 591–600. [CrossRef]
6. Khan, W.A.; Culham, J.R.; Yovanovich, M.M. Performance of Shrouded Pin-Fin Heat Sinks for Electronic Cooling. *J. Thermophys. Heat Transf.* **2006**, *20*, 408–414. [CrossRef]
7. Yang, K.; Chu, W.; Chen, I.; Wang, C. Experimental Investigations on Airside Performance of Heat Sinks Having Pin Fin Configurations. In Proceedings of the Twenty-Third Annual IEEE Semiconductor Thermal Measurement and Management Symposium, San Jose, CA, USA, 18–22 March 2007; pp. 208–212.
8. Oh, Y.W.; Choi, Y.S.; Ha, M.Y.; Min, J.K. A numerical study on the buoyancy effect around slanted-pin fins mounted on a vertical plate (Part-I: Laminar natural convection). *Int. J. Mass Transf.* **2019**, *132*, 731–744. [CrossRef]
9. Elnaggar, M.H.A.; Edwan, E. Heat Pipes for Computer Cooling Applications. In *Electronics Cooling*; Intech Open Science: London, UK, 2016; Chapter 4, pp. 52–73. [CrossRef]
10. Luo, Q.; Guan, Z.; Mao, Y.; Xiao, W.; Zeng, W. Research on Flat Heat Pipes Used in the Heat Dissipation of Laptop. *China Steel Focus* **2021**, *5*, 33–34.
11. Kim, K.-S.; Won, M.-H.; Kim, J.-W.; Back, B.J. Heat pipe cooling technology for desktop PC CPU. *Appl. Therm. Eng.* **2003**, *23*, 1137–1144. [CrossRef]
12. Mansouri, N.; Zaghlol, A.; Weasner, C. Characterization of an Embedded Heat Pipe Heat Sink for Multiple Heat sources for power electronics applications. In Proceedings of the 18th IEEE Intersociety Conference on Thermal and Thermomechanical Phe-nomena in Electronic Systems, Las Vegas, NV, USA, 28–31 May 2019. No. 675.
13. Wrobel, R.; Hussein, A. A Feasibility Study of Additively Manufactured Heat Guides for Enhanced Heat Transfer in Electrical Machines. *IEEE Trans. Ind. Appl.* **2020**, *56*, 205–215. [CrossRef]
14. Nakkaew, S.; Chitipalungsri, T.; SeonAhn, H.; Jerng, D.; Asirvatham, L.G.; SelimDalkılıç, A.; Mahian, O.; Wongwises, S. Application of the heat pipe to enhance the performance of the vapor compression refrigeration system. *Case Stud. Therm. Eng.* **2019**, *15*. [CrossRef]

15. Sun, H.; Lin, B.; Lin, Z.; Zhu, Y. Experimental study on a novel flat heat pipe heating system integrated with phase change material and thermoelectric unit. *Energy* **2019**, *189*, 116181. [CrossRef]
16. Zhang, T.; Yan, Z.W.; Xiao, L.; Fu, H.D.; Pei, G.; Jic, J. Experimental, study and design sensitivity analysis of a heat pipe photovoltaic/thermal system. *Appl. Therm. Eng*. **2019**, *162*, 114318. [CrossRef]
17. Siricharoenpanich, A.; Wiriyasart, S.; Srichat, A.; Naphon, P. Thermal management system of CPU cooling with a novel short heat pipe cooling system. *Case Stud. Therm. Eng*. **2019**, *15*, 100545. [CrossRef]
18. Kang, S.W.; Tsai, M.C. Development and Application of Heat Pipe and Vapor Chamber Heat Spreader. *J. Ind. Mater.* **2011**, *293*, 111–118.
19. Mansouri, N.; Zaghlol, A.; Weasner, C. Force Convection Performance of the Heat Sink with Embedded Heat Pipes Comparing Two Embedding Technologies for Heat Pipes. In Proceedings of the 2020 19th IEEE Intersociety Conference on Thermal and Thermomechanical Phenomena in Electronic Systems (ITherm), Orlando, FL, USA, 21–23 July 2020.